

Comparative study of Al_2O_3 and HfO_2 for surface passivation of $\text{Cu}(\text{In,Ga})\text{Se}_2$ thin-films: An innovative $\text{Al}_2\text{O}_3/\text{HfO}_2$ multi-stack design

Romain Scaffidi, Dilara G. Buldu, Guy Brammertz, Jessica de Wild, Thierry Kohl, Gizem Birant, Marc Meuris, Jef Poortmans, Denis Flandre, Bart Vermang*

R. Scaffidi, Prof. Denis Flandre
ICTEAM
UCLouvain

Place du Levant 3/L5.03.02 1348 Louvain-la-Neuve

Email address: romain.scaffidi@uclouvain.be; romain.scaffidi@gmail.com

R. Scaffidi, D. G. Buldu, Dr. G. Brammertz, T. Kohl, Dr. J. de Wild, G. Birant, Dr. M. Meuris, Prof. B. Vermang
Imec division IMOMEC (partner in Solliance)
Wetenschapspark 1, Diepenbeek 3590, Belgium

R. Scaffidi, D. G. Buldu, Dr. G. Brammertz, T. Kohl, Dr. J. de Wild, G. Birant, Dr. M. Meuris, Prof. J. Poortmans, Prof. B. Vermang
EnergyVille
Thorpark, Poort Genk 8310 & 8320, Genk 3600, Belgium

D. G. Buldu, Dr. G. Brammertz, T. Kohl, Dr. J. de Wild, G. Birant, Dr. M. Meuris, Prof. J. Poortmans, Prof. B. Vermang
Institute for Material Research (IMO)
Hasselt University (partner in Solliance)
Wetenschapspark 1, Diepenbeek 3590, Belgium

Prof. J. Poortmans
imec (partner in Solliance)
Kapeldreef 75, Leuven 3001, Belgium

Prof. J. Poortmans
Department of Electrical Engineering
KU Leuven
Kasteelpark Arenberg 10, Heverlee 3001, Belgium

Keywords: CIGS interface passivation, Al_2O_3 , HfO_2 , multi-stack, thin-film photovoltaics

In $\text{Cu}(\text{In,Ga})\text{Se}_2$ (CIGS) thin-film solar cells, interface recombination is one of the most important limiting factors with respect to device performances. Therefore, in this study, Metal-Insulator-Semiconductor samples are used to investigate and compare the passivation effects of Al_2O_3 and HfO_2 at the interface with CIGS. Capacitance-Voltage-Frequency measurements allow to qualitatively and quantitatively assess the existence of high negative charge density ($Q_f \sim -10^{12} \text{ cm}^{-2}$) and low interface-trap density ($D_{it} \sim 10^{11} \text{ cm}^{-2} \text{ eV}^{-1}$). At the

rear interface of CIGS solar cells, these respectively induce field-effect and chemical passivation. A trade-off is highlighted between stronger field-effect for HfO_2 and lower trap density for Al_2O_3 . This motivates the usage of Al_2O_3 to induce chemical passivation at the front interface of CIGS solar cells but raises the issue of its processing compatibility with the buffer layer. Therefore, an innovative $\text{Al}_2\text{O}_3/\text{HfO}_2$ multi-stack design is proposed and investigated for the first time. Effective chemical passivation is similarly demonstrated for this novel design, suggesting potential decrease in recombination rate at the front interface in CIGS solar cells and increased efficiency. 300°C annealing in N_2 environment enable to enhance passivation effectiveness by reducing D_{it} while surface cleaning may reveal useful for alternative CIGS processing methods.

1. Introduction

Solar power is now widely accepted as a strong candidate in tomorrow's cleaner energy network, replacing conventional fossil fuel-based energies and reducing the emission of greenhouse gases.^[1] With laboratory efficiencies approaching 25 % and the potential use of a variety of rigid or flexible substrates, $\text{Cu}(\text{In,Ga})\text{Se}_2$ (CIGS) solar cells are expected to largely contribute to the development of building integrated photovoltaics.^[1]

Still, active research needs to be undertaken in order to further increase the performance of CIGS-based cells and more particularly reduce their voltage deficit.^[1] Solving this issue should inevitably consider the electrical losses due to non-radiative recombination mechanisms, especially important at the interfaces. The solution investigated here relies on applying passivation strategies similar to the ones pursued in the Silicon industry, e.g. passivated emitter and rear cell (PERC).^[2-5] This method consists in integrating dielectric layers at the interfaces most affected by carrier recombination so as to mitigate the impact on performance.

Passivation has already been widely investigated and used at both interfaces in CIGS solar cells and with different dielectric materials such as Al_2O_3 ,^[6-12] HfO_2 ,^[8,13-15] and GaO_x .^[16] This

strategy allows overall enhancements of electrical performance, and more generally efficiency. Indeed, such metallic oxides enable to reduce the density of interface traps (D_{it}) and the related recombination losses at the concerned interface, i.e. by 1 to 2 orders of magnitude as compared to a full metal contact.^[17] At the same time, the surface density of fixed charges (Q_f) present at the oxide/CIGS interface produces an electrical field potentially diminishing minority carrier concentration and hence recombination, depending on the charge sign and the concerned interface.

The focus here is put on comparing the surface passivation effects of atomic layer deposited (ALD) oxide layers made of Al_2O_3 and HfO_2 at the interface with CIGS. This comparative study is based on Capacitance-Voltage (CV) measurements realized on Metal-Insulator-Semiconductor (MIS) structures involving both materials (Section 2.1 and 2.2). Such samples allow a simple analysis of the interface effects between oxide and CIGS layers before considering the influence of the buffer and window layers. In the view of integrating these materials for front passivation of complete solar cells and increase efficiency, an innovative $\text{Al}_2\text{O}_3/\text{HfO}_2$ multi-stack design is similarly investigated in Section 2.3, along with the influence of annealing treatments and surface cleaning.

2. Results

2.1. Field-effect passivation

2.1.1. Analysis technique

In order to quantify Q_f in the Al_2O_3 and HfO_2 layers, we inspect the measured CV curves in comparison with the “defect-free” case.^[17–19] This allows to determine the sign and magnitude of Q_f and thus assert the effectiveness of field-effect passivation depending on the interface considered, i.e. negative (resp. positive) Q_f is better suited to passivate the rear (resp. front) interface. The reference point for that comparison is the flat-band voltage (V_{fb}) which marks the onset of the depletion regime.

In the ideal situation without charged defects, V_{fb} equals the intrinsic potential difference (V_{ms}) between the **metal** contact work-function potential (V_m) and the Fermi level of the CIGS:

$$V_{ms} = V_m - \frac{1}{q} \left(\chi_{CIGS} + \frac{E_{g,CIGS}}{2} + \frac{kT}{q} \ln \left(\frac{N_A}{n_i} \right) \right) \quad [V] \quad (1)$$

in which $V_m = \phi_m/q$, with ϕ_m the work-function of the Silver contact considered equal to 4.5 eV in this work;^[20] χ_{CIGS} and $E_{g,CIGS}$ are respectively the electronic affinity and band gap of CIGS, equal to 4.36 eV and 1.18 eV;^[21] N_A is the density of shallow acceptor dopants in the CIGS layer to be determined with CV measurements; n_i is the intrinsic density of carriers in the CIGS layer and equal to $1.4 \times 10^{10} \text{ cm}^{-3}$;^[21] kT/q is the thermal energy.

In a real case, the charged defects induce a voltage shift of the CV curves. The magnitude and direction of this shift respectively determine the value and sign of the density of charges present in the oxide layer, as summarized in the following expression:

$$Q_f = C_{ox} \left(\frac{V_{ms} - V_{fb}}{q} \right) \quad [cm^{-2}] \quad (2)$$

With C_{ox} the oxide capacitance in $F \text{ cm}^{-2}$. Three different values of C_{ox} are generally considered: $C_{ox,geo}$ is the geometrical capacitance determined by the dielectric permittivity and thickness of the oxide. $C_{ox,max}$ is the maximum capacitance measured in strong accumulation, i.e. at high negative bias. $C_{ox,ext}$ is an estimation based on CV measurements.^[22] Since the two former quantities are assumed more sensitive to frequency dispersion and carrier statistics, the latter is expected to be the most reliable estimation, especially for the low dielectric thicknesses used here.^[22] Thus, only $C_{ox,ext}$ is used in the rest of this report and referred to as C_{ox} . The three unknown quantities in **Equation 1 and 2** then are N_A , C_{ox} and V_{fb} which are all estimated using CV measurements in the next section. Active field-effect passivation is generally indicated by values of Q_f of the order of 10^{12} - 10^{13} cm^{-2} .^[11-12]

2.1.2. Quantitative results

In **Figure 1(a)**, the 10 kHz measured CV curves corresponding to two MIS samples with either an **Al₂O₃** or **HfO₂** layer are depicted, along with their extracted oxide capacitance

respectively equal to $0.25 \mu\text{F cm}^{-2}$ and $0.81 \mu\text{F cm}^{-2}$. An example of graphical estimation of C_{ox} for the Al_2O_3 -based sample is shown in **Figure S1 in Supporting Information**.^[22] The shown CV curves result from a correction of the raw data for series parasitic elements, i.e. resistance and inductance.^[23] Both MIS devices exhibit a typical p-type CV behavior with the accumulation plateau slightly below the extracted oxide capacitance at -1.5 V. The accumulation to depletion transition is steeper for Al_2O_3 than for HfO_2 , suggesting slightly poorer capacitive behavior for the latter device.

The extraction of V_{fb} and N_A is here based on the slope of the linear part of $(1/C_m)^2$ vs. applied voltage,^[24] where C_m is the measured capacitance per unit area. It results in the values shown in **Figure 1(b)** which, following Equation 2, in turn correspond to values of Q_f of about $-1.4 \times 10^{12} \text{ cm}^{-2}$ and $-5.8 \times 10^{12} \text{ cm}^{-2}$ for Al_2O_3 and HfO_2 , respectively. Then, it appears that both materials present negative surface charge density as already reported,^[6-8,11,14-16,25] with a higher density for HfO_2 as compared to Al_2O_3 due to both higher oxide capacitance and flat-band voltage. Consequently, HfO_2 would most likely induce stronger field-effect passivation of the rear interface in CIGS solar cells and is our best candidate regarding this aspect.

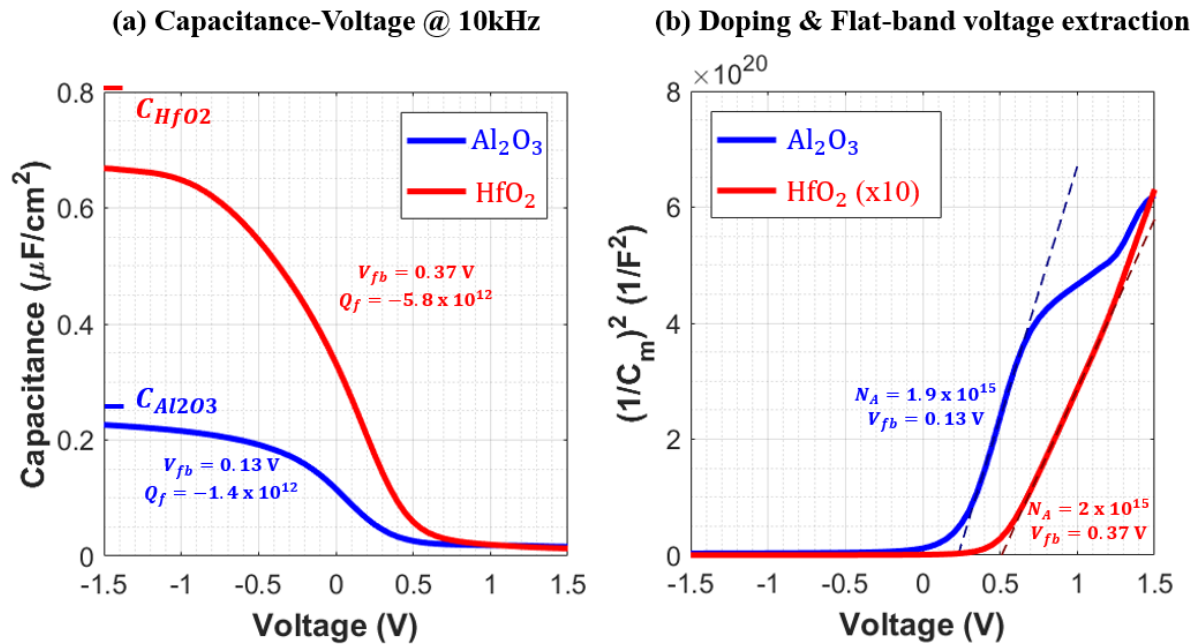


Figure 1. (a) Corrected CV curves measured at 10 kHz for MIS sample with an Al_2O_3 (blue) or HfO_2 (red) passivation layer ($C_{\text{Al}_2\text{O}_3}$ and C_{HfO_2} represent the extracted oxide capacitance of

respectively the Al_2O_3 - and the HfO_2 -based device). (b) Corresponding doping and flat-band voltage extraction. The slope of the linear part of the $(I/C_m)^2$ curve with respect to voltage is represented in dotted lines (10-fold scale-up in the case of HfO_2 for the sake of clarity). N_A is expressed in cm^{-3} and Q_f in cm^{-2} .

2.2. Chemical passivation

2.2.1. Analysis technique

In order to characterize chemical passivation effects induced by Al_2O_3 and HfO_2 at the interface with CIGS, we need to quantify the density of recombination centers (traps) at that very interface. Since these trap levels are spread along the whole interface bandgap and cannot be distinguished due to the negligible energy spacing between them, it is more practical for experimental evaluation to consider a continuous equivalent interface-trap density distribution (D_{it}) with a central energy level and expressed in $\text{cm}^{-2} \text{eV}^{-1}$.^[17]

Consequently to this approximation, only the magnitude of D_{it} can be experimentally determined and not the type of interface defects (acceptor or donor).^[17]

In practice, estimating the magnitude of D_{it} is based on the evolution of either the parallel capacitance (C) or conductance (G) with both voltage (V) and frequency (f).^[17,19] The angular frequency is here denoted ω and equal to $2\pi f$. In this work, we use the conductance method (CM) because it is less affected by parasitic elements,^[6] such as those for which the CV curves in Figure 1 were corrected. The CM relies on the fact that, for a fixed bias in the depletion regime (above V_{fb}), the curve drawn by the evolution of G/ω with respect to ω reaches a peak related to maximum energy losses induced by charge exchange with interface states.^[17-19] The height of this parallel conductance maximum is then a direct image of D_{it} , through the following simplified and straightforward expression:^[19]

$$D_{it} = \frac{2.5 * \left(\frac{G}{A\omega} \right)_{max}}{q} [\text{cm}^{-2} \text{eV}^{-1}] \quad (4)$$

in which $(G/A\omega)_{max}$ is the height of the peak observed on the G/ω vs. ω curve, normalized by the device area A and expressed in $F\text{ cm}^{-2}$. One approximation in the formula used here is the constant value of 2.5 used as correction factor for the peak width statistical fluctuations.^[19] Since the CM relies on G/ω vs. ω curves observed for voltages above flat-band (depletion), it is important to reflect about which part of the interface bandgap is inspected for such bias. Indeed, the occupation state of the interface defects depends on the interface Fermi level.^[17-19] Then, the energy band bending induced by varying the applied bias determines the depth of the traps for which D_{it} is extracted (**Figure 2**).

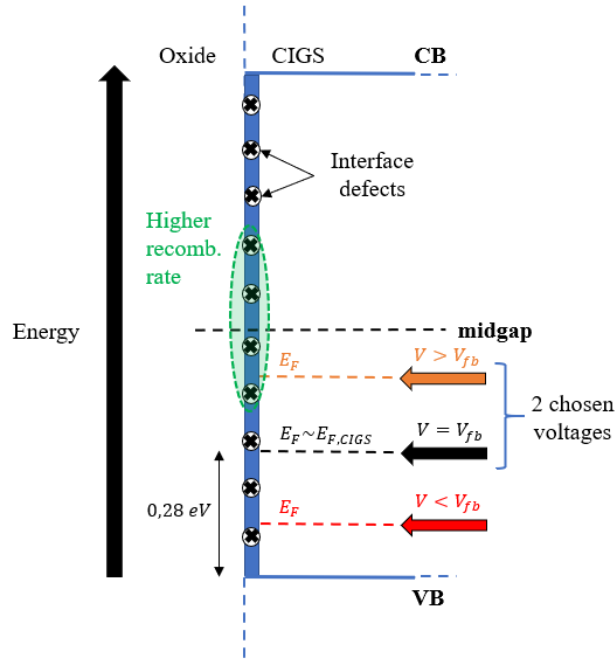


Figure 2. Idealized energy bands representation of defects characterization using the CM at the oxide/CIGS interface, highlighting the influence of applied bias on the bandgap region being inspected. VB and CB respectively stand for valence and conduction band. E_f and $E_{f,CIGS}$ respectively correspond to the interface Fermi level and the CIGS Fermi level due to p-type doping, located 0.28 eV above VB following Equation 1 and the extracted doping concentration in Figure 1.

It is visible that voltages equal to, or more positive than, V_{fb} allow to characterize the density of interface states closer to the midgap. In that region of the bandgap, interface defects induce higher surface recombination as compared to band edges, and are thus more detrimental.^[17]

Therefore, we decide to estimate D_{it} at two different voltages: (1) $V=V_{fb}$ for typical extraction

in depletion (2) $V=V_{fb}+0.5$ V to assess the density of deeper traps, i.e. with a higher incidence on recombination rate and thus electrical performance.

For our experiments, we use frequencies in the [1 kHz, 1 MHz] range, as it is typically done in practice to evaluate D_{it} .^[19] Interface-trap densities of the order of 10^{11} - 10^{12} cm⁻² eV⁻¹ usually indicate effective chemical passivation.^[6-8,11,15,25]

2.2.2. Quantitative results

The parallel conductance peaks related to interface traps are represented in **Figure 3** for the same samples as Figure 1 and the two different chosen voltages.

At $V=V_{fb}$, Figure 3(a) shows an interface defect-related maximum around 10 kHz with a magnitude close to 0.012 $\mu\text{F cm}^{-2}$ for the sample with Al_2O_3 . This in turn corresponds to a D_{it} value of about 1.8×10^{11} cm⁻² eV⁻¹, indicating effective chemical passivation at the Al_2O_3 /CIGS interface.^[6-8,11,15,25] The increase of G/ω at high-frequency is due to series resistance effects.^[26,27] The origin of this parasitic resistance may possibly be attributed to the presence of border traps in the aluminum oxide layer,^[28] or to a resistive potential barrier at the back contact.^[29] For the same bias, the HfO_2 peak is scaled up by about a factor 3 as compared to Al_2O_3 , sign of more prominent interface-trap response and density.

Quantitatively speaking, the conductance peak reaches 0.037 $\mu\text{F cm}^{-2}$ for a D_{it} value of 5.8×10^{11} cm⁻² eV⁻¹. In comparison with Al_2O_3 , this suggests weaker but still active chemical passivation effects at the HfO_2 /CIGS interface, given the orders of magnitude observed in similar structures.^[15]

At higher bias and thus for trap states closer to midgap (Figure 3(b)), D_{it} is approximately 6 (resp. 8) times lower for Al_2O_3 (resp. HfO_2) and is reduced to an order of magnitude of 10^{10} cm⁻² eV⁻¹. The same trend is typically observed when comparing the density of deeper and shallower interface states.^[17]

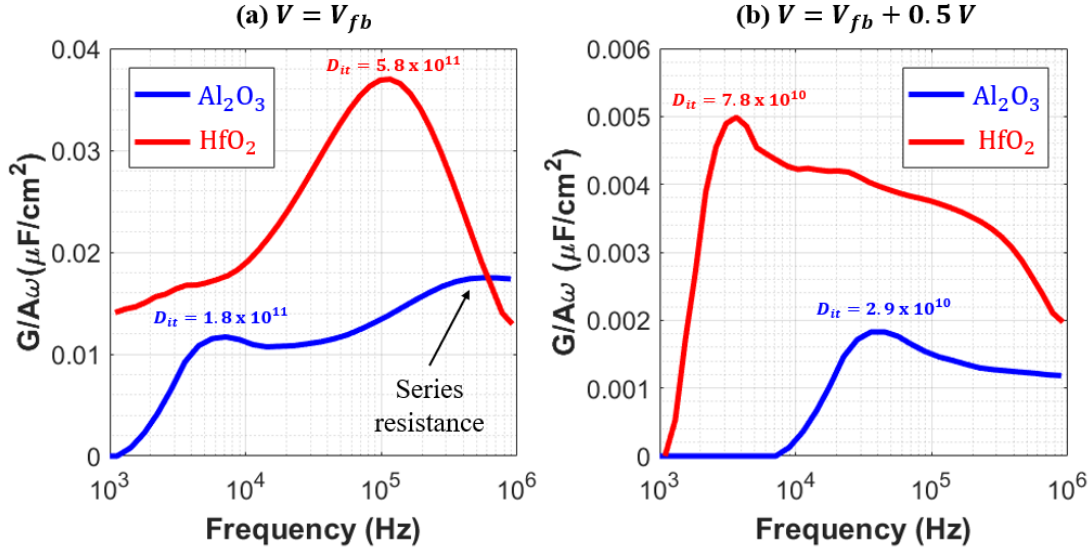


Figure 3. Parallel conductance peaks related to interface states, observed in depletion at $V = V_{fb}$ (a) and $V = V_{fb} + 0.5$ V (b), for 20nm Al_2O_3 MIS sample (blue) and 30nm HfO_2 MIS sample (red). All the curves shown result from a noise-filtering of the raw data. The values of D_{it} are expressed in $\text{cm}^{-2} \text{eV}^{-1}$.

The characterization of chemical passivation reported here tends to indicate that, over a large part of the interface bandgap, Al_2O_3 induces a more significant reduction of D_{it} than HfO_2 at the CIGS surface. Al_2O_3 is then our best candidate for mitigating the interface-trap density and related recombination losses at either one of the two interfaces in CIGS solar cells.

2.3. Multi-stack

2.3.1. Motivation

The promising passivation properties of both Al_2O_3 and HfO_2 at the interface with CIGS are compared in our CV analysis of MIS samples. The negative densities of fixed charges and low interface-trap densities observed in Al_2O_3 and HfO_2 can be used to passivate the rear interface of CIGS solar cells and enhance performance, as already reported.^[9-10,13,15] Still, we suggest also investigating the potential efficiency improvements when used at the CIGS/buffer interface. More precisely, the drastic reduction of interface-trap density ensured by Al_2O_3 , i.e. down to the order of $10^{10} \text{ cm}^{-2} \text{eV}^{-1}$ for near-midgap states, can be taken advantage of to guarantee chemical passivation of the front interface. However, this raises the

question of processing compatibility between Al_2O_3 and typical buffer layers in CIGS solar cells.

Indeed, Al_2O_3 can actually be etched by Ammonia-based solutions.^[30] Such solutions are standardly involved during the **chemical bath deposition** (CBD) of buffer layer in complete CIGS cells. Then, we need a way to protect the front Al_2O_3 passivation layer from undesired etching during the CBD step. The solution investigated here is to take advantage of hafnium oxide compounds' compatibility with Ammonia.^[30] In particular, we use an overlying HfO_2 layer to prevent the bottom Al_2O_3 layer and possible contact openings pattern to be damaged during CBD of buffer layers.

Our whole passivation layer then consists in two superimposed oxide layers of Al_2O_3 and HfO_2 , which we call the $\text{Al}_2\text{O}_3/\text{HfO}_2$ multi-stack. This novel CIGS/ $\text{Al}_2\text{O}_3/\text{HfO}_2$ configuration has the advantage of keeping interesting chemical passivation effects at the $\text{Al}_2\text{O}_3/\text{CIGS}$ interface while being compatible with solar cells production.

In the next section, we also investigate two possible methods to optimize our new design. First, applying a specific cleaning procedure on the CIGS surface before depositing the oxide may improve **the CIGS/ Al_2O_3 interface quality**. Up to this point, standard Ammonium cleaning was used as surface treatment for single-stack samples.^[30] In the following, we compare its effect on multi-stack devices with another cleaning procedure based on Ammonium Sulfide (AS) given the reported etching of undesired secondary phases,^[31] and improved electrical performances in CIGS-based devices.^[32] Second, 300°C annealing treatments in N_2 environment have a demonstrated influence on the materials composition, especially with respect to charge and interface trap distribution,^[3,4,13,33] and grain boundary.^[34] Therefore, we aim at seeing potential improvements of our multi-stack devices after application of such annealing processes.

2.3.2 Field-effect passivation

The 10 kHz measured CV curves obtained for multi-stack samples are presented in **Figure 4**, with a bias range extended to 2 V for observing a sufficient part of the depletion regime. Regardless of CIGS pre-cleaning, Q_f is negative and of the order of 10^{12} cm^{-2} before annealing. This results from the superposition of the negative charge densities intrinsically present in both dielectric layers of the stack. There is a slight difference between Ammonium and AS cleaning with respect to the measured capacitance at -1.5 V. This might be explained by a small diminution of the effective oxide thickness due to the AS treatment applied on the CIGS surface, thus affecting the actual value of C_{ox} .

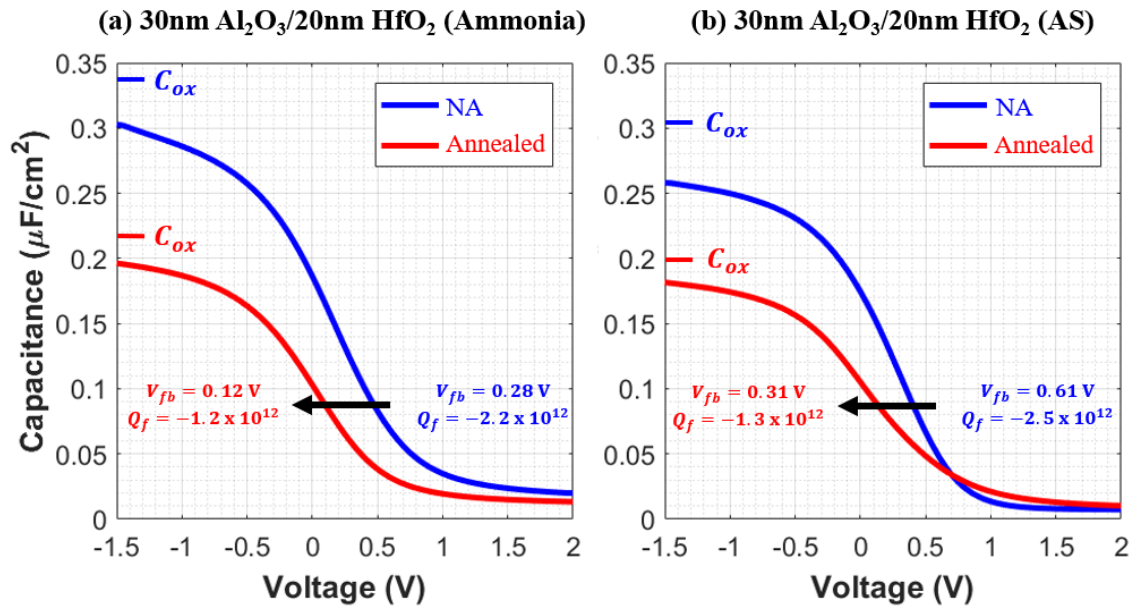


Figure 4. CV curves measured at 10 kHz for multi-stack samples, respectively pre-cleaned with Ammonia (a) and AS (b). The results for non-annealed (NA) samples (resp. 300 °C annealed samples) are represented in blue (resp. in red). The curves are shifted leftwards after the 300 °C annealing due to the modification of charges distribution within the oxide layers. The values of Q_f are expressed in cm^{-2} .

Annealing treatments at 300 °C influence the charge distribution in the $\text{Al}_2\text{O}_3/\text{HfO}_2$ stack, as well as the C_{ox} value most likely due to structural modification of the oxide layers. More precisely, the CV curves are shifted leftwards by respectively 0.16 V and 0.3 V for the sample cleaned with respectively Ammonia and AS. This corresponds to about a 50 % decrease in Q_f , as shown in Figure 4. Increasing the annealing temperature to 400 °C induces similar changes in Q_f (**Figure S2 in Supporting Information**) so that, after either 300 °C or 400 °C annealing

in N₂, the global charge distribution in the oxide layers remains negative and of the order of 10^{12} cm^{-2} .

Regardless of annealing, surface cleaning only has a slight impact on Q_f , with a variation in charge density magnitude by about 10 %. The Ammonium and AS treatment being applied on the CIGS surface, they thus have a limited influence on the charge composition within the oxide layers.

2.3.3. Chemical passivation

The conductance peaks at $V=V_{fb}$ are represented in **Figure 5**, with the voltage shift induced by annealing taken into account. The corresponding densities of interface traps D_{it} stay of the order of $10^{11} \text{ cm}^{-2} \text{ eV}^{-1}$ for multi-stack samples, indicating active chemical passivation as expected with the high quality of the Al₂O₃/CIGS interface. This is especially the case of Ammonia pre-cleaned sample with $D_{it} = 2.9 \times 10^{11} \text{ cm}^{-2} \text{ eV}^{-1}$ before annealing, as compared to the AS-treated device whose density of interface traps is about 3 times higher. Even though the AS treatment does not provide the lowest value of D_{it} in our samples, it may prove interesting to improve the quality of CIGS layers processed by one-stage co-evaporation or sputtering.^[31,32]

For both Ammonium and AS cleaning, 300 °C annealing tends to improve chemical passivation by reducing the density of recombination traps at the interface by 30 to 40 %. An opposite trend is observed in similar samples annealed at 400 °C (**Figure S3 in Supporting Information**), for which D_{it} is increased by a factor 2 after annealing.

Contrarily to the single-layered devices, the G/ω curves at $V=V_{fb}+0.5 \text{ V}$ do not exhibit clear peaks in the [1 kHz, 1 MHz] range (**Figure S4 in Supporting Information**). Still, we expect the same trend of decreasing D_{it} for deeper interface states to apply to multi-stack samples too.

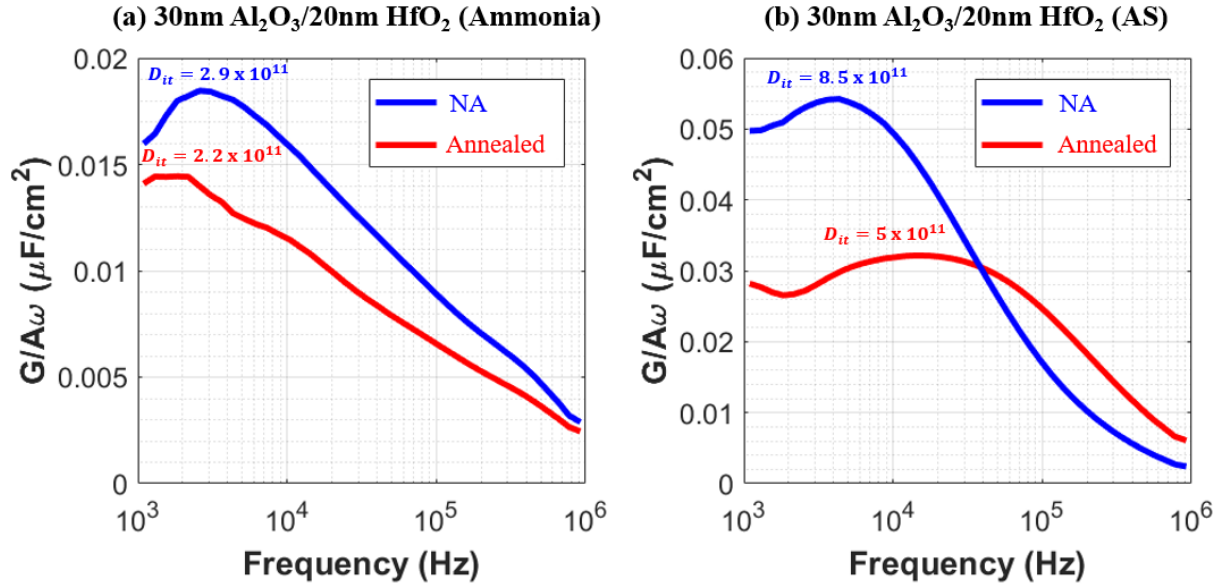


Figure 5. Parallel conductance peaks related to interface states, observed in depletion at $V=V_{fb}$, for $\text{Al}_2\text{O}_3/\text{HfO}_2$ multi-stack MIS sample treated with Ammonia (a) and AS (b). The results for NA samples (resp. 300 °C annealed samples) are represented in blue (resp. in red). For both cleaning procedures, the 300 °C annealing treatment enhances chemical passivation, i.e. D_{it} is decreased by about 30 to 40 %. All the curves shown result from a noise-filtering of the raw data. The values of D_{it} are expressed in $\text{cm}^{-2} \text{eV}^{-1}$.

3. Conclusion

Our comparative characterization of aluminum and hafnium oxide highlights their interesting and versatile surface passivation properties at the interface with CIGS ($Q_f \sim -10^{12} \text{ cm}^{-2}$ and $D_{it} \sim 10^{11} \text{ cm}^{-2} \text{eV}^{-1}$). In particular, we highlight their complementarity as possible candidates to support the development of both rear- and front-passivated CIGS solar cells.

Indeed, at the Mo/CIGS interface where negative charges create a beneficial back electrical field, either Al_2O_3 or HfO_2 can be used with a tradeoff between stronger field-effect for HfO_2 and lower interface-trap density for Al_2O_3 .

At the CIGS/buffer interface where positive charges would be more appropriate to reduce minority carrier concentration, Al_2O_3 is the best choice given its both lower negative Q_f and D_{it} . However, Al_2O_3 alone is not compatible with the typical deposition technique of buffer layer involved in CIGS solar cells. Therefore, we propose and characterize an innovative $\text{Al}_2\text{O}_3/\text{HfO}_2$ multi-stack passivation design in which HfO_2 is used to protect the underlying

Al_2O_3 layer from undesired etching during buffer processing. The very low interface-trap density expected with Al_2O_3 is attested by our CV characterization of multi-stack devices. This suggests likely improvements of electrical performance in CIGS solar cells using our novel configuration as front passivation stack.

For the $\text{Al}_2\text{O}_3/\text{HfO}_2$ multi-stack, Ammonium surface cleaning leads to lower values of D_{it} as compared to AS treatment. Still, the latter procedure may reveal interesting to apply on CIGS layers deposited and/or grown differently than for our samples. Regardless of CIGS cleaning, N_2 annealing treatments at 300 °C have the positive effect of decreasing D_{it} . Eventually, our most effective multi-stack design regarding chemical passivation is the one with Ammonium-based CIGS cleaning and 300 °C annealing in N_2 , for which D_{it} is about $2.2 \times 10^{11} \text{ cm}^{-2} \text{ eV}^{-1}$. The proposed multi-stack structure may be further optimized with regards to the thicknesses of the two oxide layers. Moreover, the potential association of this $\text{Al}_2\text{O}_3/\text{HfO}_2$ configuration with the patterning of contact-openings is presently under investigation with encouraging results.

4. Experimental Section

Samples processing: The general layout of our samples is depicted in **Figure 6**. The front contact consists in a 200nm-thick square lattice made of thermally evaporated Silver, with a contact area of 0.01 cm^2 per device. The oxide passivation stack is either single-layered (20 nm Al_2O_3 or 30 nm HfO_2) or multi-stacked (30 nm Al_2O_3 /20 nm HfO_2). The Al_2O_3 (resp. HfO_2) layers are processed by the Savannah Thermal ALD tool at 300 °C (resp. 250 °C), with Trimethylaluminium (resp. Tetrakis (EthylMethylAmino) Hafnium) used as precursor and H_2O used as reactant for a rate of 0.13 nm/cycle (resp. 0.15 nm/cycle). The CIGS layers used for this project are produced by 3-stage co-evaporation with typical thickness between 1.6 μm and 1.8 μm . Their top surface is cleaned by default with Ammonia prior to the oxide deposition, but Ammonia Sulfide (AS) is used instead for some multi-stack samples (see Section 4.3). The diffusion of Na atoms towards the CIGS during its processing is ensured by

an underlying NaF-based Sodium precursor layer (omitted in Figure 6). Below lies the 300 nm-thick DC sputtered Molybdenum back electrode, resting on top of the 2–3 mm-thick soda-lime glass (SLG) substrate. The CIGS layers present a notch-type Gallium grading, with CGI and GGI ratios respectively comprised within the [0.75, 0.9] and [0.3, 0.34] ranges. In this work, we performed annealing processes with a duration of 30 minutes for the high-temperature plateau at either 300 or 400 °C, and under constant N₂ flow.^[3,4,13,33] The annealing itself is performed inside the ATV PEO601 fast ramping furnace, with the following sequence:

1. Initialization: 2 minutes of hold time under N₂ flow
2. Heating up: 10 minutes of heating up to respectively reach 300 °C or 400 °C under N₂ flow
3. Annealing: 30 minutes of thermal annealing at 300 °C or 400 °C under N₂ flow
4. Cooling down: 20 minutes of cooling down to respectively reach 300 °C or 400 °C under N₂ flow

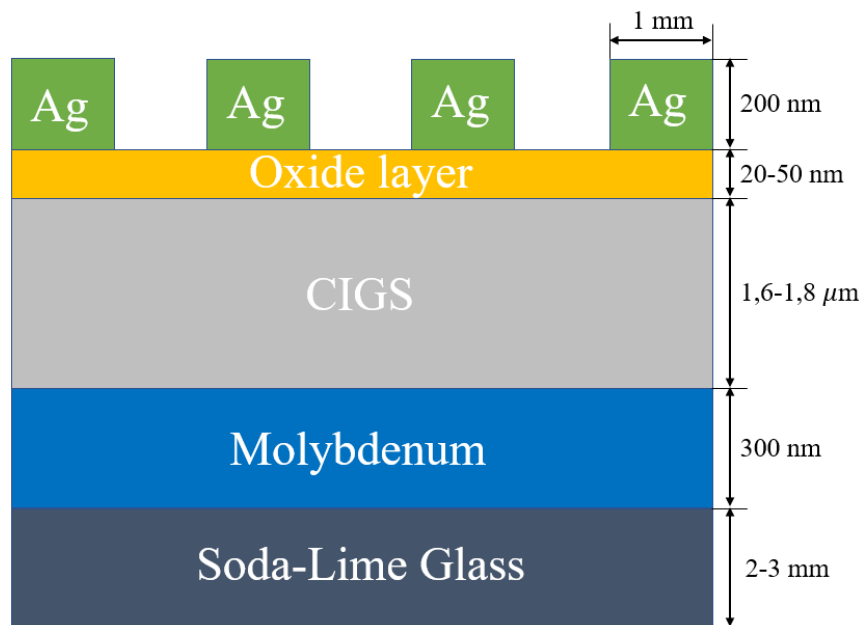


Figure 6. Schematic representation of the MIS structures processed for this work (approximate scale). The Sodium Fluoride precursor layer is not represented.

Capacitance-Voltage measurements: These experiments are performed on the Agilent E4980A Precision LCR meter with a 4-probe configuration. Capacitance-Voltage

measurements are realized at a fixed frequency of 10 kHz and over the $[-1.5 \text{ V}, 1.5 \text{ V}]$ or $[-1.5 \text{ V}, 2 \text{ V}]$ ranges for respectively single-stack and multi-stack samples, with 61 and 71 data points in linear voltage sweep. Capacitance-frequency measurements are realized at fixed bias of either V_{fb} or $V_{fb}+0.5 \text{ V}$ and over the $[1 \text{ kHz}, 1 \text{ MHz}]$ range, with 41 data points in logarithmic frequency sweep. The amplitude of the AC small-signal is always equal to 50 mV.

Cleaning procedure: The CIGS layers in the samples studied here are by default cleaned with Ammonia,^[31] as commonly used in surface treatment of III/V devices. Nevertheless, one objective of this study is to compare the effect of Ammonia and Ammonium Sulfide cleaning on the CIGS/oxide interface quality (D_{it}) for the multi-stack samples.^[30-32] Therefore, multi-stack samples have been processed with the exact same configuration except from the CIGS surface cleaning applied before the oxide deposition being made with either $\text{NH}_3 \cdot \text{H}_2\text{O}$ (Ammonia) or $(\text{NH}_4)_2\text{S}$ (Ammonium Sulfide). The two cleaning procedures used in this study are the following:

- $\text{NH}_3 \cdot \text{H}_2\text{O}$ cleaning
 - 6 minutes dipping into 30 % $\text{NH}_3 \cdot \text{H}_2\text{O}$ solution
 - 3 minutes rinsing into deionized water (2x)
- $(\text{NH}_4)_2\text{S}$ cleaning
 - 5 minutes dipping into $(\text{NH}_4)_2\text{S}$ solution with 6.5-7 % Sulfur concentration
 - 2 minutes rinsing into deionized water (2x)

Supporting Information

Supporting Information is available from the Wiley Online Library or from the author.

Acknowledgements

This work received funding from the European Union's H2020 research and innovation program under grant agreement No. 715027.

Received: ((will be filled in by the editorial staff))

Revised: ((will be filled in by the editorial staff))

Published online: ((will be filled in by the editorial staff))

References

- [1] G.M. Wilson, M. Al-Jassim, W.K. Metzger, S.W. Glunz, P. Verlinden, G. Xiong, L.M. Mansfield, B.J. Stanbery, K. Zhu, Y. Yan, J.J. Berry, A.J. Ptak, F. Dimroth, B.M. Kayes, A.C. Tamboli, R. Peibst, K. Catchpole, M.O. Reese, C.S. Klinga, P. Denholm, M. Morjaria, M.G. Deceglie, J.M. Freeman, M.A. Mikofski, D.C. Jordan, G. Tamizhmani, D.B. Sulas-Kern, *J. Phys. D: Appl. Phys.* **2020**, *53*, 493.
- [2] B. Vermang, H. Goverde, L. Tous, A. Lorenz, P. Choulat, J. Horzel, J. John, J. Poortmans, R. Mertens, *Prog. Photovolt.* **2012**, *20*, 269.
- [3] A. Morato, B. Vermang, H. Goverde, E. Cornagliotti, G. Meneghesso, J. John, J. Poortmans, presented at *38th IEEE PVSC*, Austin, TX, June **2012**.
- [4] X. Cheng, R. Päivikki, H. Halvard, A. Perros, E. Marstein, M. Di Sabatino, H. Savin, *IEEE J. Photovolt.* **2017**, *7*, 1.
- [5] R. Kotipalli, R. Delamare, O. Poncelet, X. Tang, L. Francis, D. Flandre, *EPJ Photovolt.* **2013**, *4*, 1.
- [6] R. Kotipalli, *Surface Passivation Effects of Aluminum oxide on Ultra-Thin CIGS Solar Cells*, Université Catholique de Louvain, Belgium **2015**.
- [7] R. Kotipalli, O. Poncelet, G. Li, Y. Zeng, L. Francis, B. Vermang, D. Flandre, *Sol. Energy* **2017**, *157*, 603.
- [8] D. Ledinek, O. Donzel-Gargand, M. Sköld, J. Keller, M. Edoff, *Sol. Energy Mat. Sol. Cells* **2018**, *187*, 160.
- [9] B. Vermang, V. Fjällström, J. Pettersson, P. Salomé, M. Edoff, *Sol. Energy Mat. Sol. Cells* **2013**, *117*, 505.
- [10] M. Edoff, W.-C. Chen, I. Gordon, B. Vermang, P. Bolt, J. van Deelen, M. Simor, D. Flandre, J. Lontchi, M. Kovacic, J. Krc, L. Guillard, S. Collin, N. Naghavi, M. Jubault, R. Kotipalli, L. Fourdrinier, Y. Zhou, R. Vignal, V. Gusak, E. Niemi, K. Takei, S. Bose, J. Cunha, T. Lopes, P. Fernandes, P. Anacleto, S. Sadewasser, P. Salomé, presented at *36th EU PVSEC*, Marseille, September **2019**.

- [11] W.-W. Hsu, J. Chen, T.-H. Cheng, S. Lu, W.-S. Lo, Y.-Y. Chen, Y.-J. Chien, C. Liu, *Appl. Phys. Lett.* **2012**, *100*, 023508.
- [12] R. Kotipalli, B. Vermang, J. Joel, R. Rajkumar, M. Edoff, D. Flandre, *AIP Adv.* **2015**, *5*, 107101.
- [13] D. Ledinek, J. Keller, C. Hägglund, W.-C. Chen, M. Edoff, *Thin Solid Films* **2019**, *683*, 156.
- [14] J. Löckinger, S. Nishiwaki, B. Bissig, G. Degutis, Y. Romanyuk, S. Buecheler, A. Tiwari, *Sol. Energy Mat. Sol. Cells* **2019**, *195*, 213.
- [15] G. Birant, J. Mafalda, R. Scaffidi, J. de Wild, D. Buldu, T. Kohl, G. Brammertz, M. Meuris, J. Poortmans, B. Vermang, *EPJ Photovolt.* **2020**, *11*, 10.
- [16] S. Garud, N. Gampa, T.G. Allen, R. Kotipalli, D. Flandre, M. Batuk, J. Hadermann, M. Meuris, J. Poortmans, A. Smets, B. Vermang, *Phys. Status Solidi A* **2018**, *215*, 1700826.
- [17] S. Sze, K. Ng, *Physics of Semiconductor Devices*, Wiley, Hoboken, NJ **2006**.
- [18] J.-P. Colinge, C. Colinge, *Physics of Semiconductor Devices*, Kluwer Academic Publishers, Boston, MA **2002**.
- [19] E. Nicollian, J. Brews, *MOS (Metal Oxide Semiconductor) Physics and Technology*, Wiley, Hoboken, NJ **2003**.
- [20] M. Nardone, Y. Patikirige, C. Walkons, S. Bansal, T. Friedlmeier, K. Kweon, J. Varley, V. Lordi, presented at *45th IEEE PVSC*, Waikoloa, HI, June **2018**.
- [21] A. Dweydari, C. Mee, *Phys. Status Solidi A* **1975**, *27*, 223.
- [22] L. Black, *New Perspectives on Surface Passivation: Understanding the Si–Al₂O₃ Interface*, Australian National University, April **2015**.
- [23] W.H. Wu, B.Y. Tsui, Y.P. Huang, F.C. Hsieh, M.C. Chen, Y.T. Hou, Y. Jin, H.J. Tao, S.C. Chen, M.S. Liang, *IEEE Electron Device Lett.* **2006**, *27*, 399.
- [24] K. Piskorski, H. M. Przewlocki, presented at *33rd International Convention MIPRO*, Opatija, May **2010**.

- [25] J. Cunha, P. Fernandes, A. Hultqvist, J. Teixeira, S. Bose, B. Vermang, S. Garud, D. Buldu, J. Gaspar, M. Edoff, J. Leitão, P. Salomé, *IEEE J. Photovolt.* **2018**, 8, 1313.
- [26] R. Scaffidi, *Characterization of CIGS/Oxide interface passivation for Cu(In,Ga)Se₂ solar cell applications*, Université Catholique de Louvain, Belgium, September **2020**.
- [27] G. Brammertz, A. Alian, H. Lin, M. Meuris, M. Caymax, W.-E. Wang, *IEEE Trans. Electron Devices* **2011**, 58, 3890.
- [28] Y.-C. Lin, Y.-T. Hsieh, C.-M. Lai, H.-R. Hsu, *J. Alloys Compd.* **2016**, 661, 168.
- [29] J. Oh, J. Myoung, J. Bae, S. Lim, *J. Electrochem. Soc.* **2011**, 158, D217.
- [30] B. Canava, J. Vigneron, A. Etcheberry, D. Guimard, J.-F. Guillemoles, D. Lincot, S. Ould Saad Hamatly, Z. Djebbour, D. Mencaraglia, *Thin Solid Films* **2002**, 403-404, 425.
- [31] M. Buffière, A.-A. El Mel, N. Lenaers, G. Brammertz, A. Zaghi, M. Meuris, J. Poortmans, *Adv. Energy Mat.* **2014**, 5, 1.
- [32] D. G. Buldu, J. de Wild, T. Kohl, G. Brammertz, G. Birant, M. Meuris, J. Poortmans, B. Vermang, *Phys. Status Solidi A* **2020**, 217, 2000307.
- [33] J. Frascaroli, G. Seguni, E. Cianci, D. Saynova, J. van Roosmalen, M. Perego, *Phys. Status Solidi A* **2013**, 210, 732.
- [34] A.S. Pugalenth, R. Balasundaraprabhu, S. Prasanna, S. Habibuddin, N. Muthukumarasamy, G. Mohan Rao, M.D. Kannan, *Opt. Mater.* **2016**, 62, 132.

The versatility of Al₂O₃ and HfO₂ as potential passivation layers for CIGS solar cells is demonstrated. Either Al₂O₃ or HfO₂ can be used to passivate the rear interface, with a tradeoff between stronger field-effect for HfO₂ and lower interface-trap density for Al₂O₃. Chemical passivation of the front interface is suggested possible with an innovative Al₂O₃/HfO₂ multi-stack design.

Romain Scaffidi*, Dilara G. Buldu, Guy Brammertz, Jessica de Wild, Thierry Kohl, Gizem Birant, Marc Meuris, Jef Poortmans, Denis Flandre, Bart Vermang

Comparative study of Al₂O₃ and HfO₂ for surface passivation of Cu(In,Ga)Se₂ thin-films: An innovative Al₂O₃/HfO₂ multi-stack design

